Mechanistic Characterization of the HDV Genomic Ribozyme: A Mutant of the C41 Motif Provides Insight into the Positioning and Thermodynamic Linkage of Metal Ions and Protons†

Shu-ichi Nakano‡ and Philip C. Bevilacqua*

Department of Chemistry, The Pennsylvania State University, University Park, Pennsylvania 16802

Received August 23, 2006; Revised Manuscript Received December 30, 2006

ABSTRACT: Binding of two Mg^{2+} and two H^+ ions influences the self-cleavage activity of the genomic HDV ribozyme. The positioning of these four ligands and their thermodynamic linkage are not fully resolved. Protonated C41 engages in a base triple, whereas protonated C75 has been implicated as an acid−base catalyst in bond cleavage. Prior studies led to the identification of one structural inner-sphere ion and one catalytic outer-sphere ion. In the present study, the contributions of the C41 base triple to the metal ion- and pH-dependence of the reaction are examined. Experiments were conducted on a CG to UA double mutant (DM), which changes the base triple to one involving an unprotonated C41. Below pH 6, the DM has a steeper dependence on pH than the wild-type (WT), consistent with a single protonation misfolding the core; this conclusion is also supported by thermal denaturation studies. Between pH 6 and 8, the WT and DM display nearly identical catalytic metal ion and H^+ binding profiles. In contrast, over the same pH range, the WT and DM have distinct structural ion binding profiles; for the WT, binding is favored at lower pH, whereas the DM shows no pH dependence. These data localize the structural ion to the vicinity of the C41 motif. An overall model is presented that accommodates binding affinity, coupling, and positioning of the two metal ions and the two protons within the ribozyme. The data suggest that a protonated base triple allows the WT ribozyme to maintain appreciable activity at acidic pH, which could play an important role in the life cycle of the virus.

Small ribozymes are adept at using their nucleobases in catalysis (*1*). Indeed, all five known small ribozymes have been shown to react proficiently in the presence of large quantities of ethylenediaminetetraacetic acid (EDTA[1]) and monovalent ions, suggesting that divalent ions play non-essential catalytic roles (*2*−*5*). Quantitation indicates that metal ions provide only 10- to 20-fold to the rate of the hammerhead and HDV self-cleavage reactions (*4*, *6*, *7*). These observations suggest that the nucleobases participate directly in bond breaking and making events, although catalytic contributions for metal ions may also occur (*8*−*11*). Subsequent biochemical studies on these ribozymes have provided supporting evidence that nucleobases can hydrogen bond in the transition state, stabilize charge development by through-space interactions, and transfer protons as general acid−base catalysts (*3*, *12*−*17*).

The hepatitis delta virus (HDV) ribozyme is a small self-cleaving ribozyme (∼85 nt) that plays essential roles in the double rolling-circle replication of HDV (Figure 1A). Both the genomic and antigenomic forms of the virus have a ribozyme, and the two ribozymes have similar secondary structures (*18*, *19*). The ribozyme fold comprises five pairing elements (P1−P4 and P1.1) and two pseudoknots that compact the structure and provide a buried active site (Figure 1B). Ribozyme self-cleavage occurs between U-1 and G1 and leaves 5′-hydroxyl and 2′,3′-cyclic phosphate termini. No specific interactions were observed between the ribozyme and nucleotides upstream of the cleavage site in a crystal structure of the pre-cleaved ribozyme (*20*), and only one nucleotide is required upstream of the cleavage site (*21*). Self-cleavage of the ribozyme is responsible for linearizing concatemers of the genome during replication (*19*). The

† This work was supported in part by NIH Grant R01-58709.

* To whom correspondence should be addressed. Phone: (814) 863-3812. Fax: (814) 863-8403. E-mail: pcb@chem.psu.edu.

‡ Current address: Frontier Institute for Biomolecular Engineering Research (FIBER), Konan University, 8-9-1 Okamoto Higashinada-ku, Kobe 658-8501, Japan.

[1] Abbreviations: AS(−30/−7), antisense oligonucleotide targeted to the −30 to −7 stretch upstream of the self-cleavage site located between −1 and +1; C41, nucleobase that engages in a base triple with A43 and G73, which together with C44 is referred to as the quadruple motif; DM, double mutant in which C44 and G73 are changed to a U and an A, respectively; EDTA, ethylenediaminetetraacetic acid; **ER model**, electrostatic repulsion model; HEPES, 4-(2-hydroxyethyl)-1-piperazineethanesulfonic acid; **IF model**, induced fit model; inner-sphere, metal ion−RNA complex in which the ion sheds its waters of hydration to make direct contacts with the RNA; **GAB model 1**, general acid−base model for cleavage in which a hydrated magnesium ion acts as the general acid and C75 acts as the general base; **GAB model 2**, general acid−base model for cleavage in which $C75H^+$ acts as the general acid and a hydrated magnesium hydroxide acts as the general base; HDV, hepatitis delta virus; pK_a, K_a is an acid dissociation constant; K_d, a metal ion dissociation constant; k_{obs}, observed rate constant for self-cleavage; nt, nucleotide; PAGE, polyacrylamide gel electrophoresis; outer-sphere, metal ion−RNA complex in which the ion retains its waters of hydration in making direct contacts with the RNA; TE, 10 mM Tris and 1 mM EDTA (pH 7.5); TEN_{250}, TE with 250 mM NaCl; Tris, tris(hydroxymethyl)aminomethane; UV, ultraviolet; WT, wild-type ribozyme, which is in the background of the fast, monophasic G11C change.

10.1021/bi061732s CCC: $37.00
Published on Web 02/22/2007

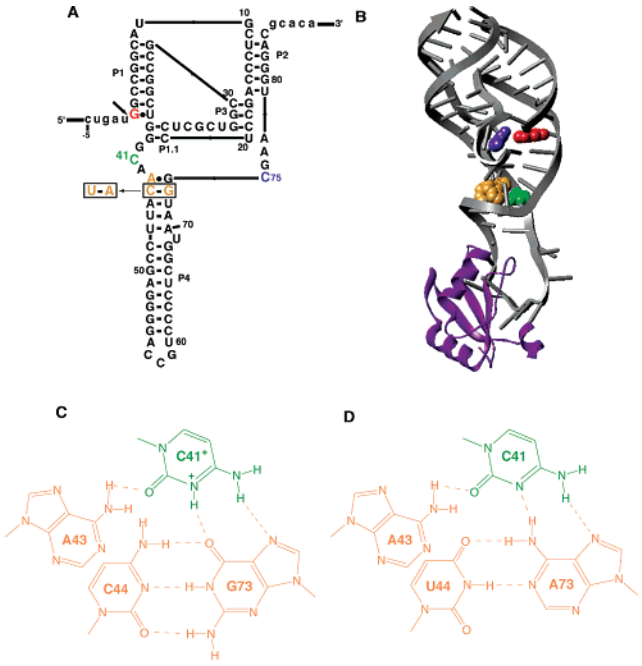

FIGURE 1: HDV ribozyme WT and DM C41 base triples. (A) Secondary structure of the HDV genomic ribozyme used in this study. Positions of importance to this study are denoted in color. The cleavage site between U-1 and G1 (red) is denoted with an arrow; C41 is shown in green, and the three other bases in the quadruple motif, A43, C44, and G73, are shown in gold; and C75, the putative general acid, is shown in blue. These colors are maintained in panel B. Position 11 has the G to C change that is a fast-folding mutant (*35*). The site of the DM C44U/G73A is indicated. (B) Positions of these bases in the crystal structure of the self-cleaved form of the ribozyme (*23*). Also shown is the U1A protein in purple. PDB file 1drz was used to create this illustration. (C) Hydrogen bonding of the bases in the WT base triple. The close distance between N3 of C41 and O6 of G73 (2.9 Å) suggests the existence of a hydrogen bond and, therefore, the protonation of the N3 of C41 (*29*). (D) Hydrogen bonding of the bases in the DM triple (*31*). The C44/G73 base pair has been replaced with a U44/A73 base pair. In this case, C41 interacts with the N6 of A73 by accepting a hydrogen bond at its N3.

reverse reaction of the ribozyme, self-ligation, has not been substantiated *in vitro*, and ligation activity *in vivo* has been assigned to a host ligase (*22*); presumably, self-ligation is inefficient because the HDV ribozyme does not have a guide sequence to pair nucleotides upstream of the cleavage site.

The HDV ribozyme is thought to bind at least four ligands: catalytic and structural divalent metal ions, and catalytic and structural protons. Evidence for these activities comes from biochemical and structural studies. Initial descriptions of the structure of the ribozyme and the pH dependence of the self-cleavage reaction implicated a nucleobase as the general base in the self-cleavage reaction (termed **GAB model 1**) (*12*, *23*). Recent crystal structures and molecular dynamic studies of the pre-cleaved state also favor **GAB model 1** (*20*, *24*, *25*). Assignment of the catalytic nucleobase to residue 75 was made on the basis of the proximity of this residue to G1 in the crystal structure of the self-cleaved ribozyme (*23*) as well as kinetic properties of a C75A mutant (*3*, *12*).

The catalytic function of C75 was interpreted differently by Nakano and co-workers, and a role as the general acid in cleavage (**GAB model 2)** was favored (*3*). This model was developed principally from two observations: (1) on the basis

Scheme 1: Three-Channel Mechanism for Ribozyme Cleavage

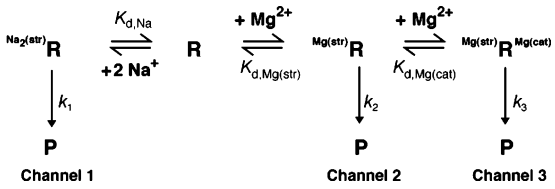

of microscopic reversibility, hydrogen bonding between the N3 of C75 and the 5′-OH of G1 in the crystal structure of the self-cleaved form of the ribozyme (*23*) implicated C75 as the proton donor in the cleavage reaction, and (2) the apparent single deprotonation pH dependence of the reaction could be recapitulated by invoking the involvement of a high pK_a species such as a hydrated magnesium hydroxide (pK_a of 11.4) as the general base in the reaction (*3*, *26*). Additional support for the involvement of an outer-sphere magnesium ion in the mechanism was found in the form of competitive inhibition by the exchange-inert $Co(NH_3)_6^{3+}$ complex (*3*) and the inversion of the rate−pH profile in the absence of Mg^{2+} (*3*, *4*). Experiments from the Piccirilli lab have provided independent support for these mechanistic assignments (*27*). In these studies, the inactive C75U mutant of the ribozyme was rescued by substituting the 5′-bridging oxygen of G1 with a sulfur atom, a much better leaving group; these results provided a molecular link between C75 and leaving group activation.

We developed a three-channel model (Scheme 1) to describe the reactivity of the ribozyme (*4*, *9*). This model was generated to account for the activity of the ribozyme in the presence of increasing concentrations of divalent ions. Channel 1 describes the reaction of the ribozyme in the absence of site-bound divalent ions and is best described as requiring two Na^+ ions to occupy the structural divalent ion site. Channel 2 involves the reaction in the presence of the structural divalent ion, whereas channel 3 involves the reaction in the presence of structural and catalytic ions. Quantitation of kinetic data according to this model provided a significant (∼125-fold) contribution of the structural ion and a modest (∼25-fold) contribution of the catalytic ion to catalysis, where fold effects were determined from the ratios of rate constants assigned to the three channels (*4*). Curiously, divalent ions were found to contribute more to folding than catalysis; indeed, the functional importance of the structural metal ion is part of the motivation for the present study.

In a follow-up study (*9*), we presented evidence that the structural metal ion has characteristics of an inner-sphere species, and the catalytic metal ion has characteristics of an outer-sphere species. Evidence for these assignments came from examining the metal dependence of self-cleavage when either channel 2 or channel 3 was dominant (*9*).[2] Under channel 2 conditions, a linear relationship was found between the inverse dehydrated ionic radius of the group IIA metal and the logarithm of its binding affinity; Na^+ competitively inhibited divalent ion binding, and the outer-sphere ion mimic

[2] The flow down channels 2 and 3 can be controlled by altering monovalent ion concentrations. In high monovalent concentrations (∼1 M), binding of the inner-sphere ion is weakened and becomes observable (channel 2). However, in low monovalent ion concentrations (no added NaCl), binding of the inner-sphere ion is so tight that self-cleavage becomes sensitive to the binding of the outer-sphere ion.

$Co(NH_3)_6^{3+}$ did not compete. Channel 3 conditions showed the opposite behavior: a non-monotonic relationship between ionic radius and binding affinity (in fact, many diverse divalent ions are known to support self-cleavage (*28*)); no dependence of activity on Na^+ concentration; and activity competitively inhibited by $Co(NH_3)_6^{3+}$, as judged by Dixon plots (*3*). These studies did not, however, reveal the location of the structural metal ion binding site.

There are two sets of crystal structures solved for the HDV ribozyme: one of the self-cleaved (*23*, *29*) and one of the pre-cleaved ribozyme, inhibited by a C75U mutation or omission of Mg^{2+} (*20*). Crystals of both constructs were grown in the presence of a U1A protein bound to a modified P4 and were solved at resolutions at or near 2.3 Å. It is important to consider what evidence these structures provide for the two metal ions and two proton ligands. (1) Catalytic metal ion: In the case of the self-cleaved ribozyme (Figure 1B), a well-defined metal ion was not observed near the active site, although weak electron density was found (*29*). For the C75U/Mg^{2+} pre-cleaved ribozyme (pdb accession code: 1SJ3), a divalent ion was found near the scissile 5′-bridging oxygen rather than the 2′-hydroxyl of U-1. This suggested that this ion might provide a proton from one of its waters to stabilize the leaving group and thus act as the general acid for cleavage consistent with **GAB model 1**. (2) Structural metal ion: There are several metal ions found in both the self-cleaved and pre-cleaved ribozymes. However, none of these ions is close enough to potential RNA ligands to serve as the inner-sphere species suggested by our previous study (*9*); ~1.9−2.5 Å is required (*30*). (3) Catalytic proton: Protons cannot be detected directly in crystal structures at these resolutions; however, the presence of protons can be inferred by the close approach (~2−3.5 Å) of heteroatoms. Crystallographic data on a catalytic proton is ambiguous at present. The self-cleaved ribozyme revealed that both the N3 and O2 of C75 are within hydrogen-bonding distance of the O5′ of G1 (2.7 and 2.6 Å, respectively), suggestive of hydrogen bonding (*23*). The pre-cleaved structures, however, did not directly reveal the hydrogen bonding of C75: the N3 of C75U is distal to both the O5′ of G1 (general acid position) and the 2′-OH of U-1 (general base position), at heteroatom distances of 4.8 and 5.4 Å, respectively (*20*). The pre-cleaved structural model can be rotated to accommodate U75 near the 2′-OH nucleophile, which supports the **GAB model 1**. (4) Structural proton: Crystallographic data provide strong support for a proton binding to the N3 of C41. A base triple involving C41, A43, and G73 of the C44/G73 base pair (also referred to in the literature as the base quadruple motif (*29*, *31*)) is found in both the self-cleaved and pre-cleaved structures and involves the hydrogen bonding between the protonated N3-H of $C41H^+$ and the O6 of G73 (Figure 1C) (*20*, *29*). Biochemical evidence for the structural proton is strong as well and is based in part on kinetic analysis from the Been lab of a double mutant (DM) of the quadruple motif in which the 44:73 base pair is changed from a CG to a UA, which allows the base triple to form without the protonation of C41 (*31*) (Figure 1D). Additional evidence that the C41 proton does not play a direct catalytic role in the mechanism comes both from nucleotide analogue interference modifications (NAIM) studies (*32*) as well as nucleobase rescue experiments (*33*). The presence of proton binding to bases other than C41 was not suggested from the crystallographic data.

In an effort to determine the location of the structural ion and possible thermodynamic linkage among the binding of the two H^+ and two Mg^{2+} ions, we studied the kinetic properties of the C41 DM. Observation that the structural metal ion binds tighter at low pH suggested that it might sense the protonation state of C41 and, therefore, be sensitive to the nature of the C41 motif (*4*). The protonation status of C41 was modulated by changing the wild-type ribozyme to the double mutant, established in the Been laboratory (*31*) (Figure 1D). We then studied the pH and metal ion concentration dependencies of this mutant, as well as its folding stability. The data localize the structural metal ion to the vicinity of the C41 quadruple motif and support a novel role for the protonated base triple in enabling the ribozyme to maintain activity at acidic pH.

MATERIALS AND METHODS

Materials. The ribozyme was prepared and renatured as described previously (*4*, *9*, *34*). All experiments were conducted in the background of the G11C mutant of the −30/99 ribozyme (i.e., the WT has the G11C change). This is because the G11C mutation promotes a fast, monophasic reaction because of the destabilization of the Alt P1 misfold (*35*).

In general, solutions and tubes were treated with Chelex resin, as described previously (*4*). Mutant plasmids were generated from pT7-30/99 (*34*) using the QuikChange kit (Stratagene). Sequences were confirmed by the dideoxy method after miniprep purification (Qiagen) and again after maxiprep purification (Qiagen) to control for revertants.

Methods. Kinetic Methods and Data Fitting. In general, kinetic methods followed those previously described (*3*, *4*, *9*, *34*). Reactions were initiated by the addition of Mg^{2+} or a Mg^{2+}/Na^+ mixture, as appropriate, and included 10 μM AS(−30/−7) antisense oligonucleotide to resolve the Alt 1 misfold (*34*). Reactions were limited to a pH range of 4−9, outside of which acid- and alkaline-denaturation events overwhelm k_{obs} and preclude a straightforward analysis (*36*).

Plots were made using KaleidaGraph (Synergy Software) and analyzed by nonlinear curve fitting. Equations used to fit the data were derived in two ways. In the Results section, we fit the data using the simplest equations possible (provided in this section). In general, these equations were derived from schemes involving the minimal number of protonation or deprotonation events necessary to arrive at the active ribozyme species and follow directly from **GAB model 1**. Single-step additions to these schemes and equations that accommodate coupled protonation−deprotonation events and follow from **GAB model 2** are provided in Supporting Information.

Rate-pH profiles for the WT ribozyme in the presence of Mg^{2+} were fit according to the logarithm of eq 1, which comes from a kinetic model in which a single deprotonation event is needed to provide the active ribozyme species (Scheme 2); for this scheme, it is assumed that the general acid process is facilitated by a species whose functional, protonated form is present in a pH-independent amount over the experimentally accessible pH range of 4−9 such as a hydrated magnesium ion that has a pK_a of 11.4 (*37*). Both

Scheme 2: Single-Deprotonation Mechanism (**GAB Model 1**)[a]

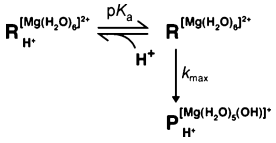

[a] H^+ depicts the protonation of a ribozyme nucleobase. Charges depicted on the product species in Schemes 2, 3, and 5 are inferred from microscopic reversibility.

k_{max} and pK_a are denoted here as observed constants because they are themselves a function of Mg^{2+} concentration, as described below.

$$k_{obs,WT} = \frac{k_{max,obs}}{1 + 10^{pK_{a,obs} - pH}} \quad (1)$$

Rate-pH profiles for the DM in the presence of Mg^{2+} were fit according to eq 2a, which is derived from a kinetic model in which two deprotonation events, with values pK_{a1} and pK_{a2}, are needed to provide the active ribozyme species (Scheme 3). Thermodynamic coupling between the two pK_a values was assumed to be zero; the experimental data support the assignment of these pK_a values to C75 and C41 as well as absence of coupling (see Results).

$$k_{obs,DM} = \frac{k_{max,obs}}{1 + 10^{pK_{a1,obs} - pH} + 10^{pK_{a2,obs} - pH} + 10^{pK_{a1,obs} + pK_{a2,obs} - 2pH}} \quad (2a)$$

The denominator of this rate−law equation can also be factored into the terms for each protonation event (*36*, *38*).

$$k_{obs,DM} = \frac{k_{max,obs}}{(1 + 10^{pK_{a1,obs} - pH})(1 + 10^{pK_{a2,obs} - pH})} \quad (2b)$$

Magnesium ion binding profiles for the WT and DM were fit according to eq 3, which can be derived from a model in which magnesium ions bind cooperatively, with a Hill coefficient of α_H and a dissociation constant of K_d, to provide the active ribozyme species (Scheme 4). Both k_{max} and K_d are denoted as observed constants because they are themselves a function of pH, as described below.

$$k_{obs} = \frac{k_{max,obs}[Mg^{2+}]^{\alpha_H}/K_{d,obs}{}^{\alpha_H}}{1 + [Mg^{2+}]^{\alpha_H}/K_{d,obs}{}^{\alpha_H}} \quad (3)$$

Coupling of Mg^{2+} and H^+ binding was accounted for by eqs 4−6, which follow from a kinetic model in which a Mg^{2+} ion binds to the ribozyme in the absence (K_{d1}) or presence (K_{d2}) of a bound proton to arrive at the single active ribozyme species (Scheme 5). Of course this scheme also describes H^+ binding to the ribozyme in the absence (pK_{a1}) or presence (pK_{a2}) of a bound magnesium ion.[3] The dependence of k_{obs} on Mg^{2+} concentration for channel 2 and channel 3 conditions could be fit well by the general hyperbolic Mg^{2+} binding equation, eq 3, with α_H set to unity to give $K_{d,obs}$ and $k_{max,obs}$, which are parametric in pH according to eqs 4 and 6, respectively. Secondary plots of log $K_{d,obs}$ as a function of pH were fit to the logarithm of eq 4 to provide the intrinsic Mg^{2+} affinity constant in the absence of bound proton, K_{d1}, and the two intrinsic pK_a values; the intrinsic Mg^{2+} affinity constant in the presence of the bound proton, K_{d2}, was obtained using eq 5 and these three values. Plots of $k_{max,obs}$ versus pH were used to confirm the value of pK_{a2} (eq 6) (not shown).

Scheme 3: Double-Deprotonation Mechanism (**GAB Model 1**)

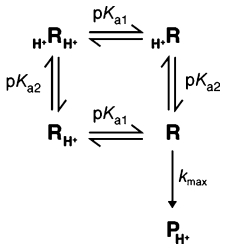

Scheme 4: Multiple-Mg^{2+} Mechanism

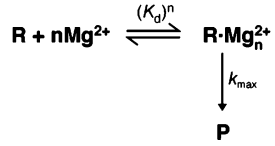

Scheme 5. Single-Deprotonation/Single-Mg^{2+} Mechanism (GAB Model 1)

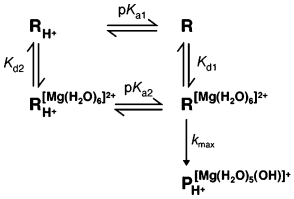

$$K_{d,obs} = K_{d1}\frac{1 + 10^{pK_{a1} - pH}}{1 + 10^{pK_{a2} - pH}} \quad (4)$$

$$K_{d2} = K_{d1} \times 10^{pK_{a1} - pK_{a2}} \quad (5)$$

$$k_{max,obs} = \frac{k_{max}K_{a2}}{K_{a2} + [H^+]} \quad (6)$$

This set of equations describes a set of k_{obs} − Mg^{2+} plots that have the same pH-dependencies for $K_{d,obs}$ and $k_{max,obs}$, as observed previously (*3*).

The kinetic model in Scheme 5 can also be used to provide a dependence of k_{obs} on pH that could be fit well by the general H^+ binding equation, eq 1, to give p$K_{a,obs}$ and $k_{max,obs}$, each of which is parametric in Mg^{2+} concentration (Supporting Information). Secondary plots of p$K_{a,obs}$ as a function of Mg^{2+} were not carried out because they would be redundant to those above. Nonetheless, it is noteworthy that this treatment leads to equations that provide a set of log k_{obs} − pH plots that have the same Mg^{2+} dependence of p$K_{a,obs}$ and $k_{max,obs}$, as observed previously (*3*).

[3] pK_{a1} and pK_{a2} from Schemes 3 and 5 are not necessarily the same pK_a values.

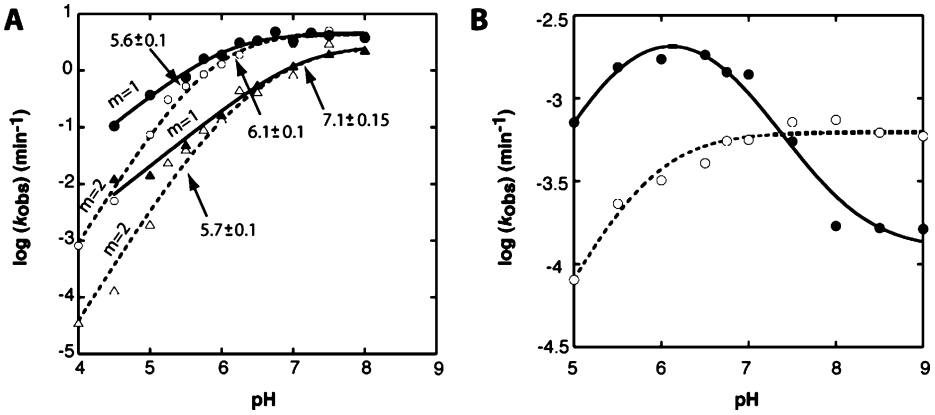

FIGURE 2: Comparison of the pH dependence for WT (filled symbols) and DM (open symbols) ribozymes. (A) Experiments conducted in the presence of 0.87 mM (△, ▲) or 10 mM (○, ●) Mg^{2+}. Data are with no added NaCl, which probe channel 3 of the mechanism. Fits to the WT (—) ($R^2 = 0.98$) were according to the logarithm of eq 1 to give k_{max} values of 2.7 ± 0.8 and 4.5 ± 0.3 min^{-1}, and pK_a, values of 7.1 ± 0.15 and 6.1 ± 0.1 at 0.87 and 10 mM Mg^{2+}, respectively. Fits to the DM (---) ($R^2 = 0.98-0.99$) were according to the logarithm of eq 2a in which the values of k_{max} and pK_{a1} were fixed according to those determined for the WT at the respective Mg^{2+} concentration (entries in the preceding sentence). This resulted in pK_{a2} values of 5.7 ± 0.1 and 5.6 ± 0.1 at 0.87 and 10 mM Mg^{2+}, respectively. Data for the WT ribozyme are from ref *3*. (B) Experiments in the presence of 1 M NaCl/100 mM Na_2EDTA, which probe channel 1 of the mechanism. Fits to the DM (---) ($R^2 = 0.98$) were according to the logarithm of eq 1 to give a k_{max} value of (6.2 ± 0.34) × 10^{-4} min^{-1} and a pK_a value of 5.8 ± 0.1. Data for the WT ribozyme are from ref *3* and are shown for comparison. Adequate description of WT data required a four-state model, whereas DM data could be well fit with a two-state model.

The coupling free energy at 37 °C ($\Delta G°_{37,C}$) in units of kcal/mol is defined by eq 7 (*36*).

$$\Delta G°_{37,C} = -1.42(pK_{a2} - pK_{a1}) \quad (7)$$

Thermodynamic Methods and Data Fitting. Self-cleaved WT and DM ribozymes were used in UV melting studies. These species were prepared by allowing the ribozyme to react to completion in the presence of AS(−30/−7) and Mg^{2+}, as previously described (*9*). RNAs were PAGE purified, eluted in TEN_{250}, precipitated with ethanol, washed with 70% ethanol, and stored in TE at −20 °C. UV melting profiles were acquired at 260 nm on a Gilford Response II spectrophotometer, as described (*9*). The reversibility of the melts and the monomeric nature of the RNA were confirmed as described (*9*). The heating rate was ∼1 °C/min, and the data were smoothed over five points before taking the first derivative. For the comparative plot in Figure 3A, the first derivatives were normalized by dividing by the absorbance at the lowest temperature after smoothing. High temperature normalizations were avoided because absorbance at these values can reflect differences in cleavage of the phosphodiester backbone (*39*).

The T_M was determined from the maximum of the first derivative of absorbance with respect to temperature. As discussed previously, this system has two melting transitions, which are well-separated, making this approach reasonable (*9*). Because melts were carried out at high concentrations of Na^+ (1 M), the second transition was too stable to measure, and we were only able to obtain the T_M for the first of the two transitions; this transition has been previously assigned to the unfolding of the tertiary structure (*9*).

RESULTS

Dependence of Activity on pH for WT and DM Ribozymes. A prior study indicated that the binding of the divalent ion under high monovalent ion conditions (1 M NaCl) is favored at lower pH (*4*). In contrast, divalent ion binding observed under low monovalent ion conditions (i.e., no added NaCl) is favored at higher pH (*3*, *4*). Because lower pH favored the binding of the structural ion, we hypothesized that it might be located near the cationic C41 quadruple motif. We, therefore, made the C44/G73 to U44/A73 double mutant ribozyme, which should form a C41 base triple without the protonation of C41 (Figure 1C, D) (*31*), and studied its kinetic properties.

The pH rate profiles for self-cleavage of the WT and DM ribozymes in the presence of no added NaCl are shown in Figure 2A. Two plots, parametric in Mg^{2+} concentration, are provided for each ribozyme. We begin by considering the higher Mg^{2+} (10 mM) plots. For the WT, log k_{obs} increased linearly with pH over the lower pH range of 4.5−6 (slope of ∼1), and reached a plateau at higher pH (6−8), as previously described (*3*). The slope of 1 in the lower pH regime is consistent with a single deprotonation activating the ribozyme, and the data can be fit well by eq 1, which follows from Scheme 2.

Over the higher pH range (5.5−8.0), the DM shows kinetics that are indistinguishable from that of the WT. Both ribozymes give the same rates in the plateau region (pH 6.5−8.0) (Figure 2A). Moreover, both ribozymes showed a similar loss of activity (slope of ∼1) with decreasing pH between ∼6.2 and 5.5. Previous studies have assigned this pK_a to C75 (*3*); thus, the similarity of the WT and DM activity between pH 5.5 and 8 suggests that the DM has little or no effect on C75 proton affinity.

In the lower Mg^{2+} (0.9 mM) plot, the WT and DM ribozymes again show virtually identical behavior between pH 5.5 and 8. Both display a slope of 1 in the low pH portion of this range and plateau at higher pH. In addition, both WT and DM curves in 0.9 mM Mg^{2+} are shifted to a higher pK_a value relative to the 10 mM Mg^{2+} curve, consistent with the anticooperative coupling previously assigned to a repulsion between $C75H^+$ and a catalytic divalent ion (*3*). The similarity of the WT and DM rate−pH profiles across different Mg^{2+} concentrations suggests that, in addition to not affecting C75 proton affinity, the DM does not signifi-

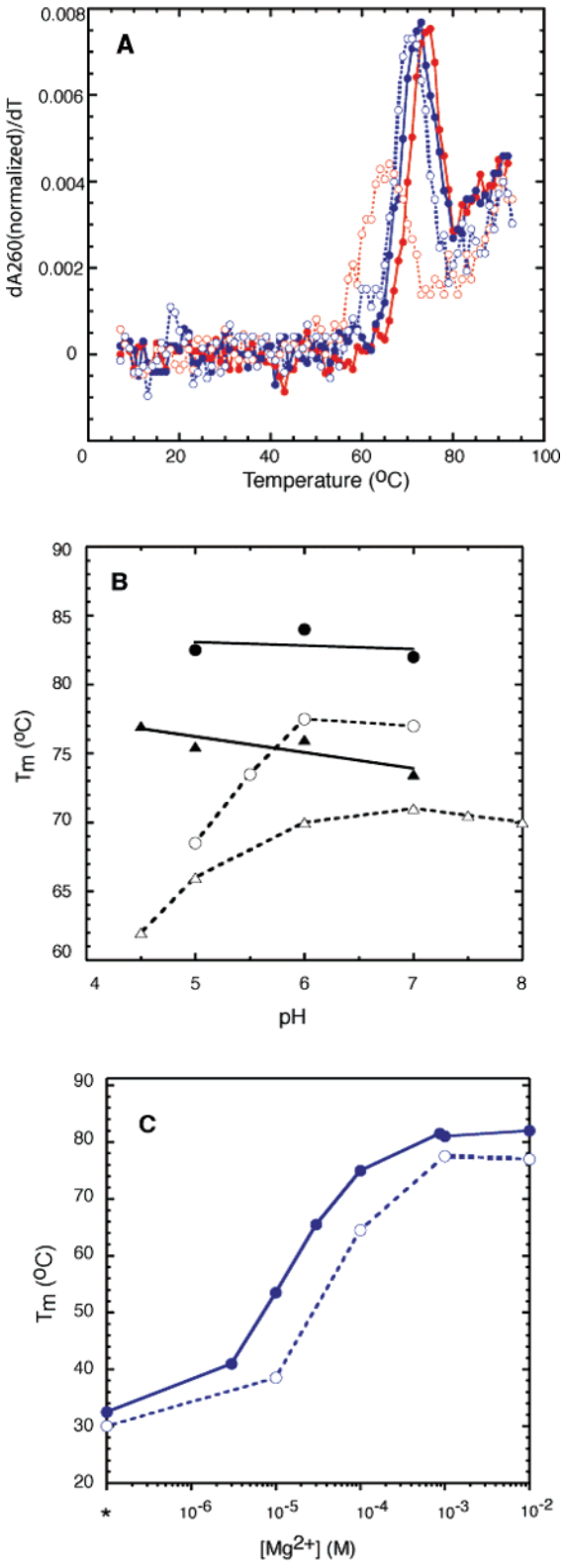

FIGURE 3: Comparison of the stability of the cleaved WT (filled symbols; solid lines) and DM (open symbols; dashed lines) ribozymes. (A) Melting profiles for the WT and DM ribozymes in 1 M NaCl at pH 5 (red) and 7 (blue). Data are colored red for acid and blue for basic to facilitate interpretation. (B) Dependence of T_m on pH for the first melting transition for WT and DM ribozymes in 1 M NaCl (△, ▲) and 10 mM Mg^{2+} (○, ●). (C) Dependence of T_m on Mg^{2+} concentration plot for WT and DM ribozymes in the absence of added NaCl at pH 7. Data with the asterisk is measured in the presence of 1 mM EDTA, and the Mg^{2+} concentration is ~10^{-7} M on the basis of our previous study (*4*); the actual value is not critical to the interpretation of the data.

cantly affect the binding of the catalytic Mg^{2+} ion (also confirmed in Figure 4A).

In contrast to the higher pH range, the DM displays kinetic behavior that is different from that of the WT over the lower pH regime. Strikingly, when the pH is lowered from 5.5 to 4.0, the DM shows a steeper loss in activity than the WT, which holds at both 0.9 and 10 mM Mg^{2+} (Figure 2A). Over this pH range, the rate−pH profile for the WT ribozyme continues to decrease with a slope of 1, whereas the profile for the DM ribozyme switches to a slope of 2. Data for the DM in Figure 2A can be well described by a model involving the double deprotonation required for activating the ribozyme (Scheme 3). (Note that there is no coupling depicted between the binding of these two protons, which are assigned to C75 and C41; see Discussion.) Analogous pH rate profiles were observed for the ribosome-catalyzed peptidyl transferase reaction and were assigned to the deprotonation of two distinct functional groups (*40*). If the k_{max} and pK_{a1} values for the DM are fixed to those for the WT, which is reasonable given the similarity of the behavior of these two RNAs between pH 5.5 and 8.0, then fitting of the DM with eq 2a provides a second pK_a with values of 5.7 ± 0.1 and 5.6 ± 0.1 at 0.9 and 10 mM Mg^{2+}, respectively. These data suggest that at low pH, the C41 base triple of the DM may be subject to a protonation event, which then drives the misfolding of the catalytic core of the ribozyme. The pK_a value of ~5.6 is slightly lower than the typical values for AC wobble pairs (*41*), consistent with the coupling to unfolding of the stable, neutral C41 base triple (see Discussion).

Next, we measured the pH dependence of the self-cleavage of the precursor WT and DM ribozymes in the absence of divalent ions. Experiments were conducted in the presence of 100 mM Na_2EDTA to ensure the complete sequestration of polyvalent ions, as well as 1 M NaCl to aid the folding of the ribozymes (*4*). As shown in Figure 2B, the DM displays distinctly different behavior than that of the WT. The WT ribozyme shows a complex dependence of log k_{obs} on pH. There is an increase in activity from pH 5 to ~5.5, plateau behavior from ~5.5 to 7.0, log-linear loss of activity from 7.0 to 8.0, and plateau behavior again from 8.0 to 9.0, as described (*4*).

In contrast, the activity of the DM in the absence of Mg^{2+} displays a relatively simple dependence of log k_{obs} on pH (Figure 2B). Rate increases log-linearly at low pH and plateaus above pH ~ 6.5. The rate−pH profile for the DM could be fit by eq 1 to give a pK_a value of 5.8 ± 0.1. The simplest interpretation of these data is that in the absence of Mg^{2+}, the $C41H^+$ base triple of the WT is destabilized because of $C41H^+$ deprotonation above pH ~ 7, whereas the neutral C41 base triple of the DM is not. According to this interpretation, the rate−pH profile inversion of the WT in the absence of Mg^{2+} does not provide evidence to support **GAB model 2**, as discussed elsewhere (*31*). However, the absence of inversion for the DM does not exclude the **GAB model 2** either because hydroxide ion could participate in a reaction channel for the DM as a specific base and offset the loss of C75 general acid, as discussed elsewhere for the WT for these low rates (*4*). According to this interpretation, the rate−pH inversion of the WT in the absence of Mg^{2+} provides evidence in support of **GAB model 2**.

Thermal Stability of the WT and DM Ribozymes. The observation that the DM lost activity more steeply than WT

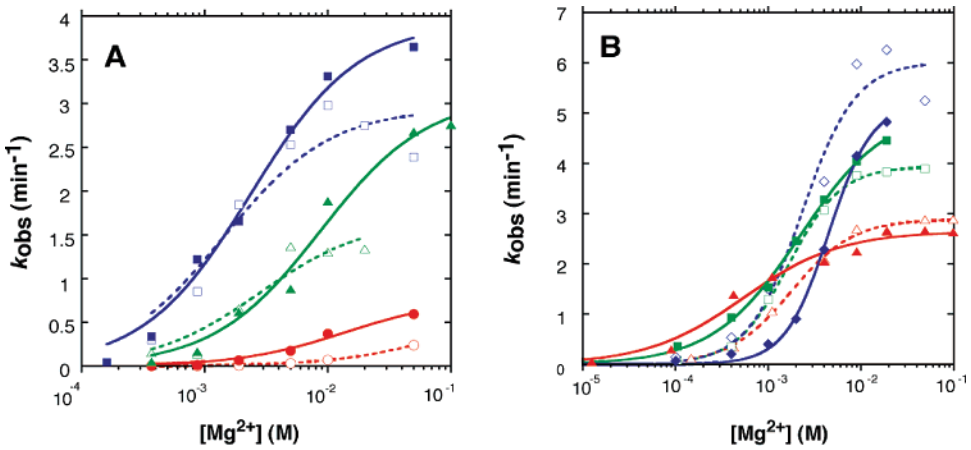

FIGURE 4: Comparison of the Mg^{2+} dependence of the WT (filled symbols; solid line fits) and DM (open symbols; dashed line fits) ribozymes at pH 5.0 (○, ●), pH 6.0 (△, ▲), pH 7.0 (□, ■), and pH 8.0 (◇, ♦). Data are colored red for acid and blue for basic to facilitate interpretation. (A) Reactivity Mg^{2+} profiles in the absence of added NaCl, which probe channel 3 of the mechanism. Fits were to a binding isotherm for a single ion, which is eq 3 in which α_H is set to 1, and the results are reported in Table 1. Data for the WT ribozyme are from ref *3*. (B) Reactivity Mg^{2+} profiles in the presence of 1 M NaCl, which probe channel 2 of the mechanism. Fits were to the Hill equation (eq 3), and the results are reported in Table 1. Data at pH 7.0 are from ref *9*.

under low pH conditions (Figure 2A), led us to investigate ribozyme folding stability. First, the stability of the self-cleaved WT and DM ribozymes was assessed in 1 M NaCl and in the absence of added divalent ions. The self-cleaved ribozymes were chosen because they should be able to reveal the influences of structural metal ions on folding. Thermal melts revealed one major unfolding transition and the beginning of another transition (at very high temperature), which have previously been assigned to tertiary structure unfolding (lower T_M) and secondary structure unfolding (higher T_M) (*9*). The T_M for secondary structure unfolding was so high that it could not be accurately determined (Figure 3A); analysis will, therefore, focus on the first T_M assigned to the tertiary structure.

As shown in Figure 3A, in 1 M NaCl the WT gave T_M values of 73.5 and 75.5 °C at pH 7 and 5, respectively. The DM, however, gave T_M values of 71.0 and 66.0 °C at pH 7 and 5, respectively. Thus, upon lowering the pH from 7 to 5, the WT showed a slight gain in stability, as expected for a protonated base-stabilized fold (*36*), whereas the DM showed a significant loss in stability. The T_M−pH data are congruent with the protonation of the DM C41 base triple[4] interfering with tertiary folding. This observation is in line with a second-order loss in self-cleavage activity for the DM with lower pH (Figure 2A). Curiously, the WT remains more stable than the DM (∼2.5 °C in T_M) at pH 7 (plateau region) despite having a positive charge at C41.

Upon carrying out melts in the presence of 10 mM Mg^{2+} (no added NaCl), similar dependencies of T_M on pH were observed, although T_M values for both ribozymes were higher relative to 1 M NaCl (Figure 3B). Upon lowering pH, the WT still showed a slight stabilization, whereas the DM gave a significant destabilization. In addition, the WT was more stable than the DM at pH 7 by ∼5 °C in T_M under these conditions.

Finally, we looked at the effect of Mg^{2+} ions on tertiary structure melting temperatures for the WT and DM ribozymes at pH 7 (Figure 3C). Over the range of $\sim 10^{-7}$−10^{-2} M Mg^{2+}, both the WT and DM were stabilized by Mg^{2+}, with similar shapes for T_M−Mg^{2+} concentration curves; however, in all instances, the DM required an ∼4-fold higher Mg^{2+} concentrations to achieve a similar T_M stabilization. These observations again support the greater thermal stability of the WT ribozyme over that of the DM and suggest that the cleaved WT binds Mg^{2+} more tightly than the DM. On the basis of the observation that between pH 6 and 8, the T_M for the DM was relatively constant (Figure 3B), we next determined the effect of pH on the affinity of catalytic and structural Mg^{2+} ions for both ribozymes.

Dependence of Activity on Mg^{2+} Concentration for WT and DM Ribozymes. The dependence of ribozyme activity on Mg^{2+} concentration was measured under conditions with no added NaCl (Figure 4A) and 1 M NaCl (Figure 4B) for both WT and DM ribozymes. For each ionic strength, three plots, parametric in pH, are provided. In the absence of added NaCl, the WT and DM display similar behavior (Figure 4A). All data are well fit by eq 3 (Scheme 4), with an α_H of 1. For both the WT and DM, K_d values for Mg^{2+} binding were lower at higher pH, with K_d values in reasonable agreement (Table 1). Because these conditions probe channel 3 of the mechanism, these observations are consistent with the DM not perturbing the binding of the catalytic Mg^{2+} ion. This observation, combined with identical pH dependencies of the WT and DM between pH 5.5 and 8.0 (Figure 2A), is consistent with the DM not significantly affecting the active site of the ribozyme.

Next, we determined the Mg^{2+} concentration dependence of self-cleavage activity in the background of 1 M NaCl for both WT and DM ribozymes (Figure 4B). Under these conditions, the WT and DM displayed strikingly different behaviors. K_d values for Mg^{2+} binding were favored at lower pH for the WT but were essentially independent of pH for the DM. For example, the K_d for Mg^{2+} binding to the WT ribozyme decreased from 4.5 to 0.5 mM as the pH decreased from 8.0 to 6.0, whereas the K_d for the DM changed from only 2.3 to 1.8 mM over the same pH range (Table 1). Curiously, the K_d for Mg^{2+} binding is ∼2-fold tighter for

[4] It is most likely that the pH dependence in the melts reflects proton binding to C41 rather than C75. This is because the WT does not show a similar low pH destabilization.

Table 1: Constants for Mg^{2+} Binding to the WT and DM Ribozymes from the Hill Equation[a]

	α_H		K_d (mM)		k_{max} (min^{-1})	
pH	WT	DM	WT	DM	WT	DM
			0 M NaCl			
5.0	1[b]	1	14 ± 3[c]	>10[d]	0.78 ± 0.07	0.63 ± 0.09
6.0	1	1	8.7 ± 1.8	2.8 ± 1.5	3.1 ± 0.2	1.7 ± 0.3
7.0	1	1	2.4 ± 0.4	1.4 ± 0.5	3.9 ± 0.2	2.9 ± 0.3
			1 M NaCl			
6.0	0.84 ± 0.12[e]	1.3 ± 0.1	0.54 ± 0.1[e]	1.8 ± 0.1	2.6 ± 0.1[e]	2.9 ± 0.1
7.0	0.92 ± 0.06	1.5 ± 0.1	2.2 ± 0.2	1.7 ± 0.1	5.1 ± 0.2	3.9 ± 0.1
8.0	1.85 ± 0.14	1.5 ± 0.5	4.5 ± 0.3	2.3 ± 0.7	5.2 ± 0.2	6.0 ± 0.5

[a] All data were fit to the Hill equation (eq 3). [b] Data for 0 M NaCl were well fit with α_H fixed at 1. [c] Thermodynamic and kinetics parameters for the WT ribozyme are from ref *3*; values with slight variation from ref *3* are due to the inclusion of a higher Mg^{2+} concentration here. [d] K_d could not be reliably determined because of a high K_d coupled with a slow rate; a lower limit for the K_d is estimated at 10 mM. [e] Thermodynamic and kinetics parameters for the WT ribozyme are from ref *4*.

the DM at pH 8.0 but ~3-fold tighter for the WT at pH 6.0. Because these conditions probe channel 2 of the mechanism, these observations are consistent with the structural metal ion sensing the protonation state of C41. Overall, the structural metal ion appears to bind weakest in the absence of a C41 base triple, intermediate in the presence of a neutral C41 triple, and strongest in the presence of a cationic C41 triple (Table 1).

Dependence of Mg^{2+} Affinity on pH for WT and DM Ribozymes. One of the striking features of the Mg^{2+} ion dependence of the WT ribozyme is that binding of the catalytic ion is favored at high pH, whereas binding of the structural ion is favored at low pH (Table 1). We developed a model that could account for these pH dependencies. Scheme 5 shows the simplest kinetic model that leads to equations able to describe this behavior. Shown are four reactant states of the ribozyme, which encompass Mg^{2+}-bound and -free, and H^+-bound and -free states. This scheme leads to eqs 3−6, in which the two intrinsic Mg^{2+} affinity constants (in the presence and absence of pH) and two intrinsic pK_a values (in the presence and absence of Mg^{2+}) can be arrived at from the pH dependence of $K_{d,obs}$ values. These four intrinsic ligand binding constants are of fundamental interest to the properties of this ribozyme.

The fit of the dependence of log K_d on pH in no added NaCl to the logarithm of eq 4 provides pK_a values for C75 of 7.25 ± 0.2 and 5.9 ± 0.1 in the absence and presence of bound Mg^{2+}, respectively. These pK_a values can be seen graphically near the flex points of the curve (Figure 5) (*36*). This analysis also provides K_d values for Mg^{2+} of 0.77 ± 0.16 and 18 ± 4 mM in the absence and presence of bound H^+, respectively. As expected, anticooperativity is manifested between the binding of the catalytic Mg^{2+} ion and the catalytic proton. The C75 pK_a value of 7.25 is intriguingly similar to the pK_a values for histidine, which is an optimal general acid−base catalyst in proteins (*42*, *43*). Representative $K_{d,obs}$ values for Mg^{2+} binding to the DM in the absence of NaCl are also displayed in Figure 5 and track those of the WT, as expected on the basis of Figure 4A.

A similar fit to eq 4 for the data in the presence of 1 M NaCl provides pK_a values of 5.5 ± 0.1 and 7.1 ± 0.1 in the absence and presence of bound Mg^{2+}, respectively. Likewise, these give K_d values for Mg^{2+} of 5.0 ± 0.3 and 0.14 ± 0.01 mM in the absence and presence of bound H^+, respectively. As expected, the coupling manifested in the K_d of the structural Mg^{2+} ion and the pK_a of C41 is favorable.

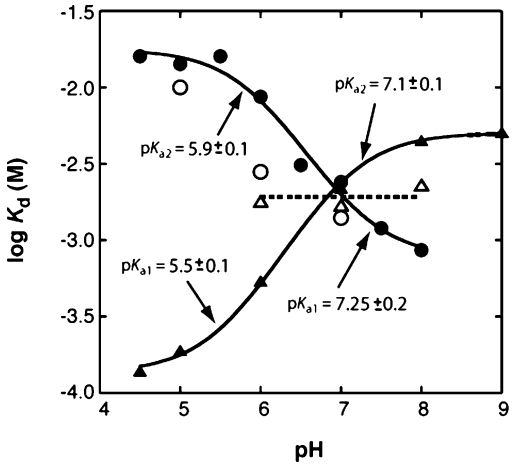

FIGURE 5: Determination of pK_a values in WT with and without bound metal ions. (●), relationship between log K_d for Mg^{2+} binding and pH in the absence of added NaCl, which probes channel 3 of the mechanism. Fit was to the logarithm of eq 4, which resulted in pK_{a2} = 5.9 ± 0.1, pK_{a1} = 7.25 ± 0.2, and K_{d1} = 0.77 ± 0.16 mM. The value of K_{d2} = 18 ± 4 mM was determined from these three values according to eq 5. (▲), relationship between log K_d and pH in the presence of 1 M NaCl, which probes channel 2 of the mechanism. Fit was to the logarithm of eq 4, which resulted in pK_{a2} = 7.1 ± 0.1, pK_{a1} = 5.5 ± 0.1, and K_{d1} = 5.0 ± 0.3 mM. The value of K_{d2} = 0.14 ± 0.01 mM was determined from these three values according to eq 5. Representative log K_d values as a function of pH for the DM in the absence (○) and presence (△) of 1 M NaCl are shown; the dashed line is a fit of the 1 M NaCl data to a line with a slope of zero.

Representative $K_{d,obs}$ values for Mg^{2+} binding to the DM in 1 M NaCl are also displayed in Figure 5 and, unlike those of the WT, are independent of pH, as expected from Figure 4B.

DISCUSSION

The two prevailing models for phosphodiester bond cleavage by the genomic HDV ribozyme both involve proton transfer by an outer-sphere Mg^{2+} ion species and by C75 (*3*, *20*, *25*, *27*). In addition, the binding of a noncatalytic inner-sphere Mg^{2+} ion and a noncatalytic proton are supported by biochemical, and structural and biochemical studies, respectively (*4*, *9*, *29*, *31*). In an effort to untangle the thermodynamic linkage of these four ligands, as well as provide insight into their positioning on the ribozyme, we investigated the kinetic properties of a C41 double mutant. We find that the protonation state of C41 has virtually no

effect on the binding and reactivity of the catalytic proton and Mg^{2+} ion but that it strongly modulates the binding properties of the structural Mg^{2+} ion.

Positioning of the Four Ligands on the Genomic HDV Ribozyme. There are two H^+ and two Mg^{2+} ions important to the mechanism of the HDV ribozyme. Three of the four ligands have received in-depth consideration in prior studies. There is consensus that the catalytic, outer-sphere metal ion and the catalytic proton are near the active site (*3*, *20*, *23*, *27*). Different models have been advanced as to which species serves as the general acid and general base (**GAB models 1 and 2**), and although these two models do require swapping of the positions of these acid−base species, both require the species to be near the scissile phosphate. Also, there is structural and biochemical evidence that the structural proton binds to C41 and, in so doing, stabilizes the base quadruple motif (*20*, *29*, *31*). Less clear is the positioning of the structural metal ion that has been identified from biochemical studies.

Previous studies demonstrated that the function of the structural ion can be probed by carrying out the reaction under conditions of 1 M NaCl (Channel 2 in Scheme 1), and those studies revealed that binding of this ion is favored by low pH (*4*). In the present study, binding of the structural ion was linked to the protonation of C41 rather than C75. When the C41 base triple was formed in the DM (pH ≥5.5), now neutral because of the mutation, binding of the structural ion was no longer a function of pH (Figures 4B and 5). This effect of the DM suggests that either the structural ion has ligands from the C41 quadruple motif or the formation of the quadruple motif indirectly alters the positioning of the metal ion ligands. However, the precise location of this ion is unclear at present. In the pre-cleaved ribozyme crystal structures, a divalent metal is located near the C41 motif (*20*); however, any potential RNA ligands are more than 4.9 Å away from this site. Curiously, several basic residues from the U1A protein appear to make direct contacts with the ribozyme phosphate backbone in this region (*20*). For instance, the pro-Sp oxygen of C44 is positioned 2.8 Å from the ϵ-amino group of K22. One possibility is that interactions of U1A residues have shifted this metal ion away from its native binding site.

There is biochemical evidence for the presence of a metal ion near the C41 motif. Two phosphorothioate interference studies have been conducted on the genomic HDV ribozyme, and both revealed the functional importance of the pro-Rp phosphoryl oxygens of C41 and C44 of the quadruple motif (*44*, *45*); for both interferences, ribozyme activity could be restored in part by elevating the concentration of Mg^{2+}, consistent with the involvement in metal binding (*45*). (The pro-Sp oxygens could not be assayed in these studies for technical reasons.) If the metal ion does indeed bind to the C41 quartet, it is likely positioned some distance from the cationic C41N3 itself; otherwise, negative linkage should have occurred.

Thermodynamic Linkage of the Four Ligands. The HDV genomic ribozyme displays both positive and negative heterotropic linkage depending on the Mg^{2+} and cytosine-H^+ ligand pair being considered (*46*). The negative linkage between the catalytic metal ion and H^+ is similar to that observed with the U6 RNA (*47*, *48*). The positive linkage between the structural metal ion and H^+ is paradoxical given that the two ions have the same charge. In an effort to understand these opposing H^+−Mg^{2+} linkages, we consider two physical models: an electrostatic repulsion model (**ER model**) and an induced fit model (**IF model**).

The simplest physical model for the negative linkage between the catalytic Mg^{2+} and H^+ ions is that of electrostatic repulsion (**ER model**). Such a ground-state destabilization could provide a driving force for catalysis if it were partially relieved in the transition state (*3*, *49*). Partial relief of repulsion in the transition state is reasonable because the transition state for this phosphoryl transfer reaction is thought to be synchronous (i.e., it involves bond orders of ∼0.5 in the transition state) on the basis of experiments on the HDV ribozyme (*4*, *50*) and model compounds (*51*). As such, the charge on C75 should be reduced to approximately +0.5 in the transition state. Ground-state destabilization is a catalytic feature peculiar to **GAB model 2** (Scheme 5′, Supporting Information); in fact, **GAB model 1** predicts ground state stabilization relative to the transition state (Scheme 5).

The simplest physical model for the positive linkage between the structural Mg^{2+} and H^+ ions is that of induced fit (**IF model**). The binding of the H^+ to C41 and the concomitant formation of the base quadruple motif could create a better inner-sphere metal ion binding site. This is congruent with the notion that inner-sphere metal ion sites require close positioning of negatively charged ligands, which would be unfavorable in the absence of a positive charge. As mentioned in the previous section, the absence of a strong anticooperative component between $C41H^+$ and the structural Mg^{2+} ion suggests that the two species are positioned relatively far apart. The distances between the N3 of C41 and the pro-Rp and -Sp phosphoryl oxygens of C44, which were discussed above in relation to metal binding, are 10.67 and 12.85 Å, respectively, and the metal might be perhaps another 2 Å away.

Somewhat surprisingly, the structural ion is observed to bind more tightly to the folded, cationic WT quadruple motif than to the folded, neutral DM quadruple motif. For example, the binding affinity of the structural ion to the DM deprotonated base triple is only 1.9 mM (averaged across pH 6−8; Table 1), whereas the intrinsic binding affinity to the WT protonated-triple is 0.14 mM (Figure 5) or ∼15-fold tighter. Also, the T_M for the WT is 2.5−5 °C higher than that for the DM at pH 7.0 (Figure 3A and B), and less Mg^{2+} is needed to achieve a given T_M for the self-cleaved WT than for DM (Figure 3C). One possibility for this effect, which can be accounted for in the **IF model**, is that because an inner-sphere site requires close positioning of negatively charged ligands, a cationic C41 may be better able to preorganize the site than a neutral one. This would be in line with the absence of anticooperative effects at C41 in the WT. Further investigation will be needed to fully understand the thermodynamic basis for this effect.

The two intrinsic pK_a values found were determined for each of C75 and C41 in WT (Figure 5). This is the first time that these four intrinsic pK_a values have been parsed out, and it is of interest to consider their molecular origins. The higher of the two intrinsic pK_a values are 7.25 for C75 (−Mg^{2+}) and 7.1 for C41 (+Mg^{2+}), whereas the lower of the two intrinsic pK_a values are 5.9 for C75 (+Mg^{2+}) and 5.5 for C41(−Mg^{2+}). The higher pK_a values are similar to those reported for the catalytic histidines in RNase A (*43*),

which is an excellent general acid−base catalyst, indicating that an RNA enzyme can adopt histidine-like physical properties by virtue of its local environment.

The origin of the metal-uncoupled pK_a value for C75 of 7.25, which is ~3 units higher than the unperturbed value of 4.2 (*52*), is likely electrostatic in origin and may come from an electrostatic sandwich between the anionic active site (*4*), the cationic C75, and the scissile phosphate. The origin of the modest metal-uncoupled value of 5.5 for C41, which is just 1.3 units higher than the unperturbed value, likely comes from folding interactions of C41, which in the absence of the structural metal ion are not strong and give only a modest pK_a shift.

The ΔpK_a values in the presence and absence of bound Mg^{2+} are virtually identical in magnitude for the two cytosines, giving coupling free energies with a magnitude of ~2.0 kcal/mol (eq 7). As described above, the coupling of the pK_a value for the C41 proton may have its origin in favorable metal ion binding (**IF model**), whereas the coupling of the C75 proton may have its origin in repulsion with the catalytic ion (**ER model**).

Curiously, although thermodynamic linkage was observed between $C41H^+$ and the structural Mg^{2+} ion, and between $C75H^+$ and the catalytic Mg^{2+} ion, no thermodynamic or kinetic linkage was observed between $C41H^+$ and either the catalytic Mg^{2+} ion or catalytic H^+. The DM has no apparent effect on the binding or reactivity properties of the catalytic Mg^{2+} (Figure 4A), the catalytic H^+ (Figure 2A), or the thermodynamic coupling between these species (Figures 2A and 5). The lack of functional communication between the charge on the C41 quartet motif and the active site is consistent with the long distance between these species; the distance from C41N3 to C75N3 is 14.9 Å in the self-cleaved ribozyme structure (pdb accession code: 1drz). The highly active antigenomic version of the HDV ribozyme does not have a C41 quartet, also consistent with the lack of an important functional coupling within this region of the ribozyme. The absence of coupling between these two regions of the ribozyme is noteworthy because long-range couplings (~20 Å) have been implicated in the mechanisms of protein enzymes (*53*) and other RNA enzymes (*54*). Notably, coupling between C41 and C75 is observed under suboptimal folding conditions (see below), suggesting that long-range couplings in functional RNA may be related to the presence of folding cooperativity.

Possible Selective Advantage of a Cationic C41. Mutation of the cationic C41 base triple to a neutral one in the DM does not significantly impair the reactivity of the ribozyme under physiological pH and metal ion conditions (Figure 2A). Despite this high pH functional equivalence, the C41 quartet in the genomic ribozyme is conserved as the cationic one described here. In particular, an alignment of 76 genomic isolates reveals that the C/G at positions 44:73 is invariant (Chadalavada, D. M., Cerrone-Szakal, A. L., and Bevilacqua, P. C., unpublished work). This raises the question as to why the double mutation does not arise in nature. One possibility is that because it is a double mutation, it is just rare. However, this seems unlikely given that this is the genome of an RNA virus. Another, more intriguing possibility is that the quartet serves a biological function.

The HDV ribozyme may need to function under low pH conditions. For example, virus entry into mammalian cells often involves transport in endosomes, with late endosomes having a particularly low pH of 5 (*55*). Under low ionic strength conditions and 1−10 mM Mg^{2+}, the DM ribozyme is inactivated by a second protonation event (Figure 2A, between pH 5.5 and 4.0). Moreover, under conditions of high ionic strength and low pH, the DM ribozyme is especially impaired (Figures 2B and 4B). Thus, depending on the pH and ionic strength conditions present during viral infection and replication, there may be a distinct selective advantage for the cationic wild-type C41 motif.

Structural Nature of the C41-Protonated DM and C41-Deprotonated WT States. The DM loses activity with low pH with a second-order dependence on H^+ concentration, whereas the WT does so with a first-order dependence (Figure 2A). One possible cause for this difference is that the protonation of C41 in the DM may induce the formation of a catalytically inactive triple with the imino hydrogen-bonded A43−G74 pair. The N4 and protonated N3 of C41 could hydrogen bond with the N7 and O6 of G74, respectively (not shown). This arrangement is similar to the native interactions in the WT $C41H^+$ triple, in which $C41H^+$ engages in these hydrogen-bonding interactions with the same atoms of G73 (Figure 1C). Because the O2 of C41 already pairs with the N6 of A43 in the native C41 quartet motif, the formation of the new base triple in the DM would involve simply swinging the N3 and N4 of C41 up to G74, which is already in position because it base pairs to A43. Base pairing of C41 to the major groove face of the A43−G74 base pair in the DM would likely disrupt a hydrogen-bonding interaction between the O6 of G74 and the N2 of the catalytically important G40 (*29*), presumably rendering this state catalytically inactive. Lowering of the T_M for tertiary structure unfolding of the DM at low pH (Figure 3) is consistent with such a breakage of interactions in the catalytic core of the ribozyme.

Base triple formation between $C41H^+$ and A43−G74 may be precluded in the WT because of the availability of the Hoogsteen face of G73 to interact with a protonated C41. Protonated C41 in the WT may prefer G73 over G74 because interaction with G73 may help create the structural metal ion binding site that leads to a more thermodynamically stable state. Thus, one function of the structural metal ion may be to ensure the proper folding of the catalytic core by preventing the misfolding of $C41H^+$. Also, the interaction of WT C41 with G73 does not require the abolishing of hydrogen bonding between G74 and G40.

Curiously, although ionization of the DM base triple causes a switch between catalytically active and inactive states, ionization of the WT triple does not. As shown in Figure 5, ionization of C41 in the presence of Mg^{2+} and high ionic strength gives an apparent pK_a close to neutrality. At present, the most compelling explanation for the absence of a loss of activity in low ionic strength upon deprotonation of C41 in the WT is that folding of the ribozyme is over-determined. Indeed the T_M of the tertiary structure of the self-cleaved WT ribozyme in just 100 μM Mg^{2+} is near 75 °C (*9*). Unlike C41 in the DM, where the gain of a proton may lead to a new (inactive) structure, the loss of a proton in the WT C41 may not lead to new interactions. The nearby guanines at positions 73 and 74 both have their Watson−Crick faces tied up in hydrogen bonding, precluding interaction with C41, whereas the interaction with the Hoogsteen face of guanines

is unfavorable in the absence of cytosine protonation. That ribozyme function is insensitive to C41 deprotonation under native conditions is also supported by NAIM experiments on the HDV genomic ribozyme, which found only one functionally important cytosine protonation, that of C75 (*32*).

Often, stable molecular networks will collapse if enough interactions are removed. This has been observed both in simple DNAs, such as triloop and tetraloop hairpins (*56*, *57*), as well as large ribozymes (*58*). That WT C41 deprotonation may lead to a loss of function only in the absence of structure-stabilizing interactions is consistent with the observation from Been and co-workers that an abasic site at C75 makes ribozyme self-cleavage sensitive to deprotonation at C41 (*33*).

It is notable that the shape of the log K_d−pH curve in Figure 5 is fully consistent with the structural metal ion binding at elevated pH, albeit weaker, despite the loss of the base triple. If there were not a structural metal ion binding site present at elevated pH, then the curve would not level off at high pH, as noted for pH-folding relationships (*36*). Thus, although the formation of the C41 quadruple motif aids metal binding, it is not essential, supporting the absence of a loss of activity upon the deprotonation of WT C41 in the presence of Mg^{2+}.

Interestingly, the same conclusion is reached for the low pH arm of the log K_d−pH curve for the catalytic ion. If there were not a catalytic metal ion binding site at low pH, then the curve would not level off at low pH. The presence of the catalytic metal site in the presence of a bound proton at C75 is fully consistent with **GAB model 2**.

ACKNOWLEDGMENT

We thank Craig Cameron for helpful conversations on virus replication, and Durga Chadalavada for help with sequence alignments. We also thank Durga Chadalavada, Barbara Golden, Andrea Szakal, and Rieko Yajima for helpful comments on the manuscript, and Andrea Szakal for checking the equations.

NOTE ADDED AFTER ASAP PUBLICATION

This manuscript was released ASAP on February 22, 2007 with typographical errors in figure captions 2 and 3. The correct version was released on February 26, 2007.

SUPPORTING INFORMATION AVAILABLE

Overview and rationale, single-deprotonation/single-Mg^{2+} mechanism (GAB model 1), single-protonation/single-deprotonation mechanism (GAB model 2), and single-protonation/single-deprotonation/single-Mg^{2+} mechanism (GAB model 2). This material is available free of charge via the Internet at http://pubs.acs.org.

REFERENCES

1. Bevilacqua, P. C., and Yajima, R. (2006) Nucleobase catalysis in ribozyme mechanism, *Curr. Opin. Chem. Biol. 10*, 455−464.
2. Murray, J. B., Seyhan, A. A., Walter, N. G., Burke, J. M., and Scott, W. G. (1998) The hammerhead, hairpin and VS ribozymes are catalytically proficient in monovalent cations alone, *Chem. Biol. 5*, 587−595.
3. Nakano, S., Chadalavada, D. M., and Bevilacqua, P. C. (2000) General acid-base catalysis in the mechanism of a hepatitis delta virus ribozyme, *Science 287*, 1493−1497.
4. Nakano, S., Proctor, D. J., and Bevilacqua, P. C. (2001) Mechanistic characterization of the HDV genomic ribozyme: assessing the catalytic and structural contributions of divalent metal ions within a multichannel reaction mechanism, *Biochemistry 40*, 12022−12038.
5. Roth, A., Nahvi, A., Lee, M., Jona, I., and Breaker, R. R. (2006) Characteristics of the glmS ribozyme suggest only structural roles for divalent metal ions, *RNA 12*, 607−619.
6. Curtis, E. A., and Bartel, D. P. (2001) The hammerhead cleavage reaction in monovalent cations, *RNA 7*, 546−552.
7. O'Rear, J. L., Wang, S., Feig, A. L., Beigelman, L., Uhlenbeck, O. C., and Herschlag, D. (2001) Comparison of the hammerhead cleavage reactions stimulated by monovalent and divalent cations, *RNA 7*, 537−545.
8. Wang, S., Karbstein, K., Peracchi, A., Beigelman, L., and Herschlag, D. (1999) Identification of the hammerhead ribozyme metal ion binding site responsible for rescue of the deleterious effect of a cleavage site phosphorothioate, *Biochemistry 38*, 14363−14378.
9. Nakano, S., Cerrone, A. L., and Bevilacqua, P. C. (2003) Mechanistic characterization of the HDV genomic ribozyme: classifying the catalytic and structural metal ion sites within a multichannel reaction mechanism, *Biochemistry 42*, 2982−2994.
10. Osborne, E. M., Schaak, J. E., and Derose, V. J. (2005) Characterization of a native hammerhead ribozyme derived from schistosomes, *RNA 11*, 187−196.
11. Martick, M., and Scott, W. G. (2006) Tertiary contacts distant from the active site prime a ribozyme for catalysis, *Cell 126*, 309−320.
12. Perrotta, A. T., Shih, I., and Been, M. D. (1999) Imidazole rescue of a cytosine mutation in a self-cleaving ribozyme, *Science 286*, 123−126.
13. Kuzmin, Y. I., Da Costa, C. P., and Fedor, M. J. (2004) Role of an active site guanine in hairpin ribozyme catalysis probed by exogenous nucleobase rescue, *J. Mol. Biol. 340*, 233−251.
14. Kuzmin, Y. I., Da Costa, C. P., Cottrell, J. W., and Fedor, M. J. (2005) Role of an active site adenine in hairpin ribozyme catalysis, *J. Mol. Biol. 349*, 989−1010.
15. Han, J., and Burke, J. M. (2005) Model for general acid-base catalysis by the hammerhead ribozyme: pH-activity relationships for G8 and G12 variants at the putative active site, *Biochemistry 44*, 7864−7870.
16. Zhao, Z. Y., McLeod, A., Harusawa, S., Araki, L., Yamaguchi, M., Kurihara, T., and Lilley, D. M. (2005) Nucleobase participation in ribozyme catalysis, *J. Am. Chem. Soc. 127*, 5026−5027.
17. Wilson, T. J., Ouellet, J., Zhao, Z. Y., Harusawa, S., Araki, L., Kurihara, T., and Lilley, D. M. (2006) Nucleobase catalysis in the hairpin ribozyme, *RNA 12*, 980−987.
18. Lai, M. M. (1995) The molecular biology of hepatitis delta virus, *Annu. Rev. Biochem. 64*, 259−286.
19. Shih, I. H., and Been, M. D. (2002) Catalytic strategies of the hepatitis delta virus ribozymes, *Annu. Rev. Biochem. 71*, 887−917.
20. Ke, A., Zhou, K., Ding, F., Cate, J. H., and Doudna, J. A. (2004) A conformational switch controls hepatitis delta virus ribozyme catalysis, *Nature 429*, 201−205.
21. Perrotta, A. T., and Been, M. D. (1991) A pseudoknot-like structure required for efficient self-cleavage of hepatitis delta virus RNA, *Nature 350*, 434−436.
22. Wadkins, T. S., and Been, M. D. (2002) Ribozyme activity in the genomic and antigenomic RNA strands of hepatitis delta virus, *Cell. Mol. Life Sci. 59*, 112−125.
23. Ferre-D'Amare, A. R., Zhou, K., and Doudna, J. A. (1998) Crystal structure of a hepatitis delta virus ribozyme, *Nature 395*, 567−574.
24. Krasovska, M. V., Sefcikova, J., Spackova, N., Sponer, J., and Walter, N. G. (2005) Structural dynamics of precursor and product of the RNA enzyme from the hepatitis delta virus as revealed by molecular dynamics simulations, *J. Mol. Biol. 351*, 731−748.
25. Krasovska, M. V., Sefcikova, J., Reblova, K., Schneider, B., Walter, N. G., and Sponer, J. (2006) Cations and hydration in catalytic RNA: molecular dynamics of the hepatitis delta virus ribozyme, *Biophys. J. 91*, 626−638.
26. Bevilacqua, P. C. (2003) Mechanistic considerations for general acid-base catalysis by RNA: Revisiting the mechanism of the hairpin ribozyme, *Biochemistry 42*, 2259−2265.
27. Das, S. R., and Piccirilli, J. A. (2005) General acid catalysis by the hepatitis delta virus ribozyme, *Nat. Chem. Biol. 1*, 1−8.

28. Suh, Y. A., Kumar, P. K., Taira, K., and Nishikawa, S. (1993) Self-cleavage activity of the genomic HDV ribozyme in the presence of various divalent metal ions, *Nucleic Acids Res. 21*, 3277−3280.
29. Ferre-D'Amare, A. R., and Doudna, J. A. (2000) Crystallization and structure determination of a hepatitis delta virus ribozyme: Use of the RNA-binding protein U1A as a crystallization module, *J. Mol. Biol. 295*, 541−556.
30. Juneau, K., Podell, E., Harrington, D. J., and Cech, T. R. (2001) Structural basis of the enhanced stability of a mutant ribozyme domain and a detailed view of RNA-solvent interactions, *Structure 9*, 221−231.
31. Wadkins, T. S., Shih, I., Perrotta, A. T., and Been, M. D. (2001) A pH-sensitive RNA tertiary interaction affects self-cleavage activity of the HDV ribozymes in the absence of added divalent metal ion, *J. Mol. Biol. 305*, 1045−1055.
32. Oyelere, A. K., Kardon, J. R., and Strobel, S. A. (2002) pK(a) perturbation in genomic hepatitis delta virus ribozyme catalysis evidenced by nucleotide analogue interference mapping, *Biochemistry 41*, 3667−3675.
33. Perrotta, A. T., Wadkins, T. S., and Been, M. D. (2006) Chemical rescue, multiple ionizable groups, and general acid−base catalysis in the HDV genomic ribozyme, *RNA 12*, 1282−1291.
34. Chadalavada, D. M., Knudsen, S. M., Nakano, S., and Bevilacqua, P. C. (2000) A role for upstream RNA structure in facilitating the catalytic fold of the genomic hepatitis delta virus ribozyme, *J. Mol. Biol. 301*, 349−367.
35. Chadalavada, D. M., Senchak, S. E., and Bevilacqua, P. C. (2002) The Folding pathway of the genomic hepatitis delta virus ribozyme is dominated by slow folding of the pseudoknots, *J. Mol. Biol. 317*, 559−575.
36. Moody, E. M., Lecomte, J. T., and Bevilacqua, P. C. (2005) Linkage between proton binding and folding in RNA: A thermodynamic framework and its experimental application for investigating pKa shifting, *RNA 11*, 157−172.
37. Feig, A. L., and Uhlenbeck, O. (1999) The Role of Metal Ions in RNA Biochemistry, in *The RNA World*, (Gesteland, R. F., Cech, T. R., and Atkins, J. F., Eds.) 2nd ed., pp 287−319, Cold Spring Harbor Laboratory Press, Cold Spring Harbor, New York.
38. Knitt, D. S., and Herschlag, D. (1996) pH dependencies of the Tetrahymena ribozyme reveal an unconventional origin of an apparent pKa, *Biochemistry 35*, 1560−1570.
39. Draper, D. E., Bukhman, Y. V., and Gluick, T. C. (2000) Thermal Methods for the Analysis of RNA Folding Pathways, in *Current Protocols in Nucleic Acid Chemistry* (Beaucage, S. L., Bergstrom, D. E., Glick, G. D., and Jones, R. A., Eds.) pp 11.3.1−11.3.13, John Wiley & Sons, New York.
40. Okuda, K., Seila, A. C., and Strobel, S. A. (2005) Uncovering the enzymatic pKa of the ribosomal peptidyl transferase reaction utilizing a fluorinated puromycin derivative, *Biochemistry 44*, 6675−6684.
41. Bevilacqua, P. C., Brown, T. S., Nakano, S., and Yajima, R. (2004) Catalytic roles for proton transfer and protonation in ribozymes, *Biopolymers 73*, 90−109.
42. Fersht, A. (1985) *Enzyme Structure and Mechanism*, 2nd ed., Freeman, New York.
43. Raines, R. T. (1998) Ribonuclease A, *Chem. Rev. 98*, 1045−1065.
44. Jeoung, Y. H., Kumar, P. K., Suh, Y. A., Taira, K., and Nishikawa, S. (1994) Identification of phosphate oxygens that are important for self- cleavage activity of the HDV ribozyme by phosphorothioate substitution interference analysis, *Nucleic Acids Res. 22*, 3722−3727.
45. Prabhu, N. S., Dinter-Gottlieb, G., and Gottlieb, P. A. (1997) Single substitutions of phosphorothioates in the HDV ribozyme G73 define regions necessary for optimal self-cleaving activity, *Nucleic Acids Res. 25*, 5119−5124.
46. Wyman, J., and Gill, S. J. (1990) *Binding and Linkage: Functional Chemistry of Biological Macromolecules*, University Science Books, Mill Valley, CA.
47. Huppler, A., Nikstad, L. J., Allmann, A. M., Brow, D. A., and Butcher, S. E. (2002) Metal binding and base ionization in the U6 RNA intramolecular stem-loop structure, *Nat. Struct. Biol. 9*, 431−435.
48. Blad, H., Reiter, N. J., Abildgaard, F., Markley, J. L., and Butcher, S. E. (2005) Dynamics and metal ion binding in the U6 RNA intramolecular stem-loop as analyzed by NMR, *J. Mol. Biol. 353*, 540−555.
49. Jencks, W. P. (1975) Binding energy, specificity, and enzymic catalysis: the circe effect, *Adv. Enzymol. 43*, 219−410.
50. Shih, I. H., and Been, M. D. (2001) Involvement of a cytosine side chain in proton transfer in the rate-determining step of ribozyme self-cleavage, *Proc. Natl. Acad. Sci. U.S.A. 98*, 1489−1494.
51. Zalatan, J. G., and Herschlag, D. (2006) Alkaline phosphatase mono- and diesterase reactions: comparative transition state analysis, *J. Am. Chem. Soc. 128*, 1293−1303.
52. Saenger, W. (1984) *Principles of Nucleic Acid Structure*, Springer-Verlag, New York.
53. Benkovic, S. J., and Hammes-Schiffer, S. (2003) A perspective on enzyme catalysis, *Science 301*, 1196−1202.
54. Rueda, D., Bokinsky, G., Rhodes, M. M., Rust, M. J., Zhuang, X., and Walter, N. G. (2004) Single-molecule enzymology of RNA: essential functional groups impact catalysis from a distance, *Proc. Natl. Acad. Sci. U.S.A. 101*, 10066−10071.
55. Smith, A. E., and Helenius, A. (2004) How viruses enter animal cells, *Science 304*, 237−242.
56. Moody, E. M., and Bevilacqua, P. C. (2003) Folding of a stable DNA motif involves a highly cooperative network of interactions, *J. Am. Chem. Soc. 125*, 16285−16293.
57. Moody, E. M., and Bevilacqua, P. C. (2004) Structural and energetic consequences of expanding a highly cooperative stable DNA hairpin loop, *J. Am. Chem. Soc. 126*, 9570−9577.
58. Kraut, D. A., Carroll, K. S., and Herschlag, D. (2003) Challenges in enzyme mechanism and energetics, *Annu. Rev. Biochem. 72*, 517−571.

BI061732S